# An Isolable Mononuclear Palladium(I) Amido Complex

Jian Liu<sup>1</sup>, Melissa M. Bollmeyer<sup>2</sup>, Yujeong Kim<sup>3,4</sup>, Dengmengfei Xiao<sup>5</sup>, Samantha N. MacMillan<sup>2</sup>, Qi Chen<sup>1</sup>, Xuebing Leng<sup>1</sup>, Sun Hee Kim<sup>3,4\*</sup>, Lili Zhao<sup>5\*</sup>, Kyle M. Lancaster<sup>2\*</sup>, and Liang Deng<sup>1\*</sup>

<sup>1</sup>State Key Laboratory of Organometallic Chemistry, Shanghai Institute of Organic Chemistry, University of Chinese Academy of Sciences, Chinese Academy of Sciences, 345 Lingling Road, Shanghai 200032, China.

**ABSTRACT:** Mononuclear Pd(I) species are putative intermediates in Pd-catalyzed reactions, but our knowledge about them is limited due to difficulties in accessing them. Herein, we report the isolation of a Pd(I) amido complex,  $[(BINAP)Pd(NHAr^{Trip})]$  (BINAP = 2,2'-bis(diphenylphosphino)-1,1'-binaphthalene,  $Ar^{Trip} = 2,6$ -bis(2',4',6'-triisopropylphenyl)phenyl), from the reaction of (BINAP)PdCl<sub>2</sub> with LiNHAr<sup>Trip</sup>. This Pd(I) amido species has been characterized by X-ray crystallography, electron paramagnetic resonance, and multi-edge Pd X-ray absorption spectroscopy. Theoretical study revealed that, while the 3-electron-2-center  $\pi$ -interaction between Pd and N in the Pd(I) complex imposes severe Pauli repulsion in its Pd–N bond, pronounced attractive inter-ligand dispersion force aids its stabilization. In accord with its electronic features, reactions of homolytic Pd–N bond cleavage and deprotonation of primary amines are observed on the Pd(I) amido complex.

## Introduction

Palladium is a frequently used metal in the modern molecular chemists' catalyst arsenal and can be found in a variety of useful organic reactions, such as Wacker oxidations, cross-couplings, C-H bond functionalization and hydrogenation reactions. Underlying the broad utility of Pd are the multiple oxidation states accessible, which suit them well to the formation and cleavage of covalent bonds. Pd compounds most commonly occur as diamagnetic, closed-shell Pd(0), Pd(II) and Pd(IV) complexes. Paramagnetic, open-shell Pd compounds are far less prevalent, but are now receiving increased attention.<sup>2-5</sup> Paramagnetic Pd(I) species, for example, are implicated as intermediates in some Pd-catalyzed reactions, but sparse data are available concerning their electronic structures and reactivity. In Pd-catalyzed C-C bond-forming reactions, Pd(I) halide species  $L_nPd^IX$  (L = phosphine; X = Br, I) are proposed to form via single-electron transfer reactions of photo-excited Pd(0) phosphine complexes with organic halides, 6-8 as well as in the reactions of Pd(0) phosphine complexes with fluoroalkyl halides (Figure 1A).9 In the reactions of Pd(0) species with dioxygen, which is a key step in Pd-catalyzed aerobic oxidation reactions, Pd(I) superoxide species  $L_n Pd^I(\eta^1 - OO^*)$  are proposed as intermediates en route to Pd(II)peroxides  $L_nPd^{II}(\eta^2-O_2)$  (Figure 1A). The formation of the Pd(I)intermediates has also been envisaged in thermolysis or photolysis of Pd(II) compounds. For example, photolysis-induced decomposition of (PNP)Pd(II) alkyl (PNP = phosphine-amido-phosphine) complexes was proposed to proceed through (PNP)Pd(I) intermediates that dimerized to yield diamagnetic, dinuclear Pd(I) complexes (Figure 1A).11

A common feature of the aforementioned reactive Pd(I) intermediates is the presence of  $\pi$ -donors—ligands whose coordinating atoms bear non-bonding lone pairs, e.g. halides, superoxide, and amido in the aforementioned cases--within Pd's inner coordination sphere. Such mononuclear Pd(I) species reported to date are exceedingly reactive and have only been observed using spectroscopic methods in γ-ray irradiated Pd(II)Cl<sub>2</sub> and Pd(II)(acac)<sub>2</sub> and thermalized Pd(II)-exchanged zeolites, 12-14 where their stability is conferred by immobilization within the lattice framework. Certain Pd(0) and Pd(II) complexes are reported to undergo chemical and electrochemical redox reactions to produce mononuclear paramagnetic Pd(I) complexes. 15-19 These include three isolable complexes  $[(PBu_3^t)_2Pd]X$ PF<sub>6</sub>,  $CB_{11}Cl_{11}H)^{18,19}$  $[(PBu_3^t)_2Pd(NCMe)](CB_{11}Cl_{11}H)^{19}$  These mononuclear Pd(I)complexes, however, are not supported

<sup>&</sup>lt;sup>2</sup>Department of Chemistry and Chemical Biology, Cornell University, Ithaca, New York 14853, United States

<sup>&</sup>lt;sup>3</sup>Western Seoul Center, Korea Basic Science Institute (KBSI), Seoul 03759, Republic of Korea.

<sup>&</sup>lt;sup>4</sup>Department of Chemistry and Nano Science, Ewha Womans University, Seoul 03760, Republic of Korea.

<sup>&</sup>lt;sup>5</sup>Institute of Advanced Synthesis, School of Chemistry and Molecular Engineering, Nanjing Tech University, Nanjing 211816, China.

<sup>\*</sup>E-mails: shkim7@kbsi.re.kr (S.H.K), ias\_llzhao@njtech.edu.cn (L.Z.), kml236@cornell.edu (K.M.L.), deng@sioc.ac.cn (L.D.)

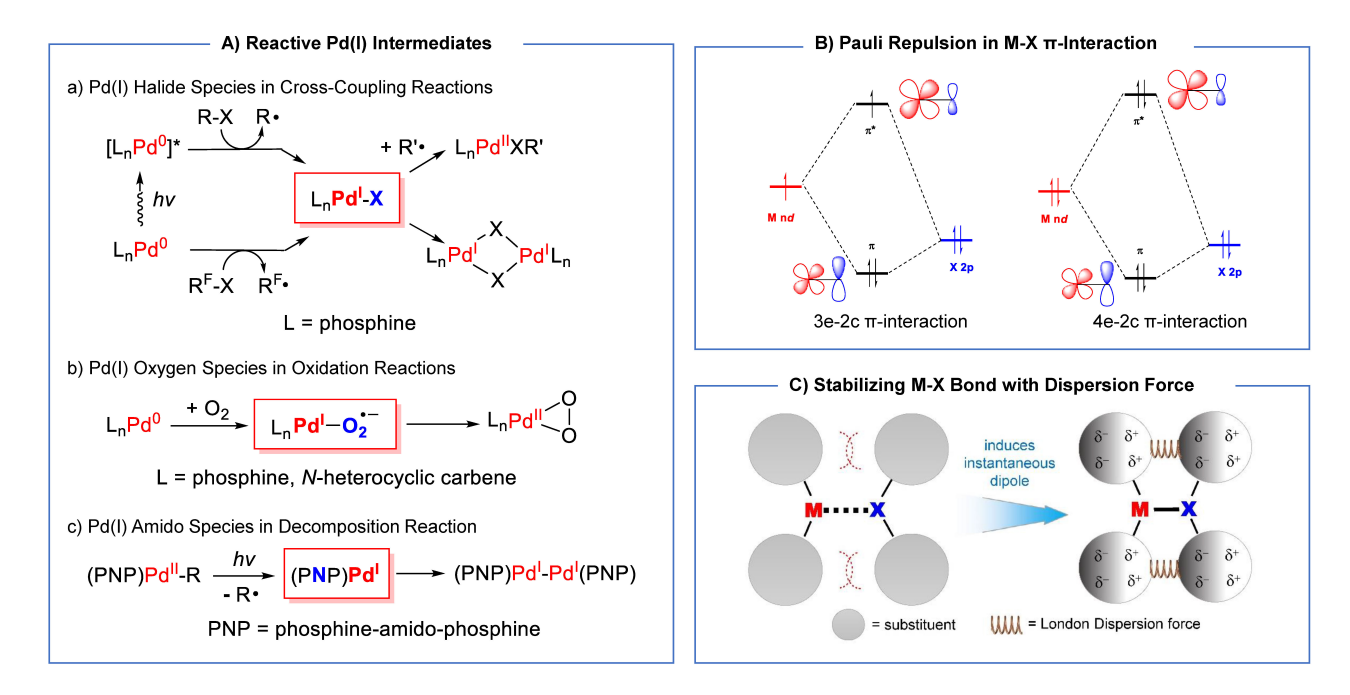


**Figure 1.** Research background on Pd(I) species bearing  $\pi$ -donating ligands. (A) Examples of reactive Pd(I) intermediates containing  $\pi$ -donating ligands. (B) Pauli repulsion in metal-ligand  $\pi$ -interaction. (C) A cartoon illustrating how London dispersion forces stabilize an M–X bond.

by  $\pi$ -donating ligands. To our knowledge, isolable Pd(I) complexes bearing  $\pi$ -donating ligand have remained elusive. The challenge of accessing mononuclear Pd(I) complexes bearing  $\pi$ -donating ligands likely originates from severe Pauli repulsion: conventional wisdom dictates that  $\pi$ -interactions between the nd orbitals of low-valent platinum-group metals (Ru, Rh, Pd, Os, Ir, Pt) and the lone pairs of  $\pi$ -donors (Figure 1B) should enforce severe Pauli repulsion, <sup>20,21</sup> leading to the destabilization of the metal–ligand multiple bond. Pauli repulsion has been used to explain the high reactivity of low-valent platinum-group metal amido, alkoxide, imido, oxo, and nitride species. <sup>22-24</sup> So far, low-valent platinum-group metal complexes containing  $\pi$ -donor ligands are restricted to the  $nd^6$ - $nd^8$  metal ions. <sup>25-27</sup> Analogous isolable complexes containing a  $nd^9$ -platinum-group metal center are unknown.

Herein we report the first nd9 platinum-group metal terminal amido complex, namely the Pd(I) complex  $[(BINAP)Pd(NHAr^{Trip})]$ (BINAP = 2,2'-bis(diphenylphosphino)-1,1'-binaphthalene, Ar<sup>Trip</sup> = 2,6-bis(2',4',6'-triisopropylphenyl) phenyl). The Pd(I) amido complex is isolated from the reaction of (BINAP)PdCl<sub>2</sub> with LiNHAr<sup>Trip</sup> and has been characterized by single-crystal X-ray diffraction, electron paramagnetic resonance spectroscopy, and multi-edge Pd X-ray absorption spectroscopy. Electronic structure calculations indicate that the Pd(I) amido complex is  $S = \frac{1}{2}$  with a three-electron twocenter π-interaction between the Pd and N atoms, and that the Pd-N bond indeed present severe destabilizing Pauli repulsion. However, dispersion forces<sup>28</sup> (Figure 1C) between BINAP and the bulky amido ligand aids the stabilization of the complex. Further reactivity studies evaluate the lability of the Pd-N bond. When subjected to thermolysis, photo-irradiation, or coordination of exogenous ligands, the Pd(I) amido complex undergoes homolytic Pd-N bond cleavage to release the aminyl radical [NHAr<sup>Trip</sup>]. In addition, the Pd(I) amido complex can react with primary alkyl and aryl amines to release NH<sub>2</sub>Ar<sup>Trip</sup>. These observations showcase the unique reactivity of low-valent, odd-electron platinum-group-metal amido complexes.

#### **Results and Discussion**

**Synthesis** and Molecular of Structure [(BINAP)Pd(NHAr<sup>Trip</sup>)]. The Pd(I)amido  $[(BINAP)Pd(NHAr^{Trip})]$  (1) was obtained via the reaction of (BINAP)PdCl<sub>2</sub> with two equivalents of LiNHAr<sup>Trip</sup>. Mixing the two reagents in toluene at -78 °C produced a blue solution, whose <sup>31</sup>P NMR spectrum features two signals with an AB-splitting pattern, suggesting the formation of a Pd(II) monoamido intermediate, presumably (BINAP)Pd(NHAr<sup>Trip</sup>)Cl (A). When warmed to room temperature, the solution turned green. Recrystallization led to the isolation of the Pd(I) amido complex  ${\bf 1}$  as a green crystalline solid in 51% yield (Figure 2A). The composition of 1 is supported by elemental analysis (C, H, N), cold electrospray mass spectroscopy (Figure S6), and its structure has been confirmed by single-crystal X-ray diffraction (Figure 2B). The infrared spectrum of 1 features an N-H stretch at 3295 cm<sup>-1</sup>. The deuterated isotopologue [(BINAP)Pd(NDAr<sup>Trip</sup>)] (1-d) shows the N-D stretch at 2538 cm<sup>-1</sup> (Figure S5). In addition to 1, three amine byproducts, the amino-imine 2, the aniline featuring an alkene side arm 3, and the free aniline 4 (Figure 2A), are observed. These amines are likely formed from the decomposition reactions of the aminyl radical [NHAr<sup>Trip</sup>]. Consequently, 1 is proposed to form via a homolytic Pd-N bond cleavage reaction of a Pd(II) bisamido intermediate,

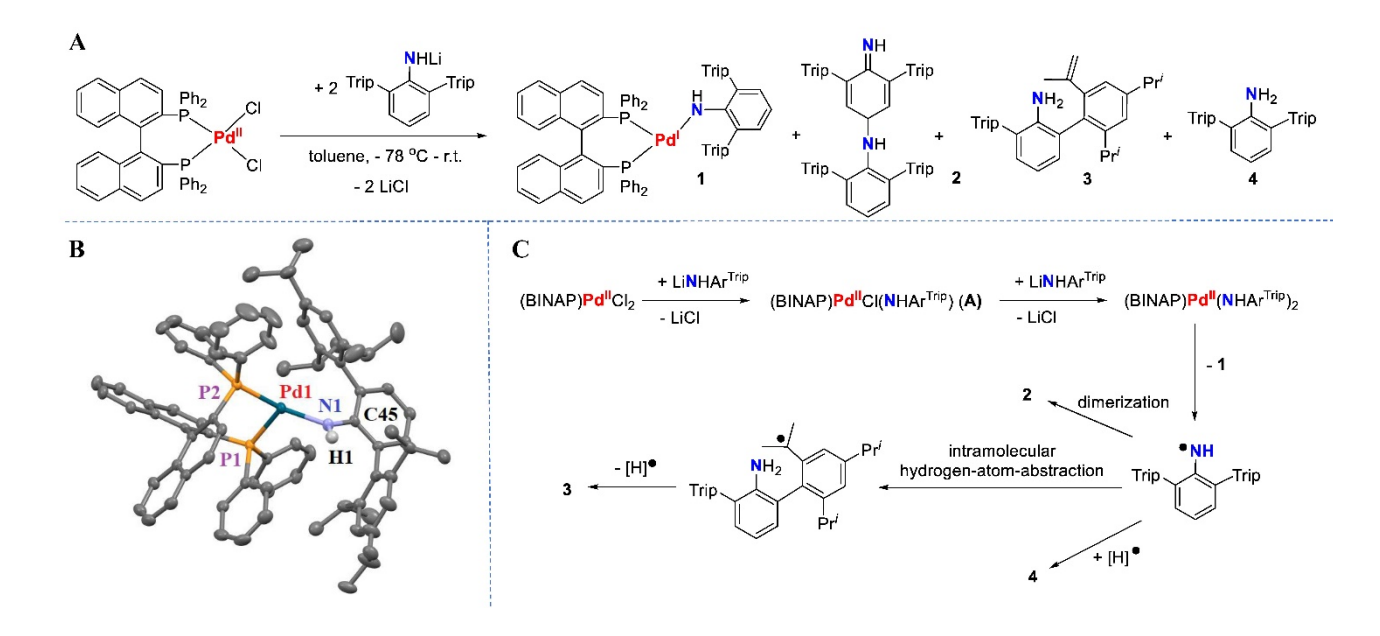
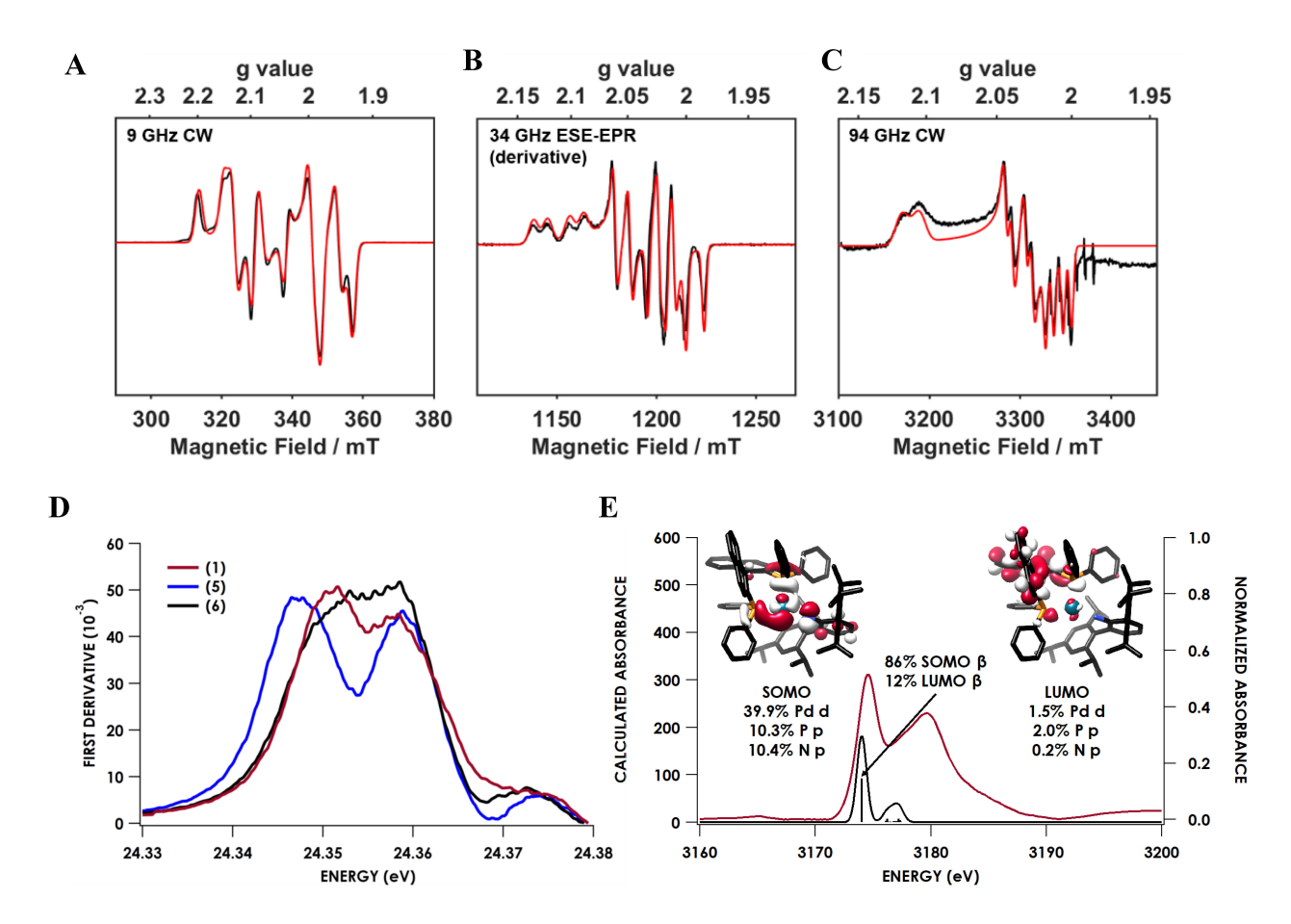


Figure 2. Synthetic route to the Pd(I) amido complex and its molecular structure. (A) The reaction giving Pd(I) amido complex  $[(BINAP)Pd(NHAr^{Trip})]$  (1) and the byproducts 2-4. (B) Molecular structure of 1, showing one of the two crystallographically independent molecules in the unit cell with 30% thermal ellipsoids and a partial atom numbering scheme. Hydrogen atoms, except the one on N1, are omitted for clarity. Selected distances (Å) and angles (deg): Pd1-N1 2.063(2), Pd1-P1 2.3314(7), Pd1-P2 2.2883(7), N1-C45 1.377(3), P2-Pd1-P1 92.20(2), Pd1-P1 108.06(6), Pd1-P2 154.04(6), Pd1-P2 154.04(6)

(BINAP)Pd(NHAr<sup>Trip</sup>)<sub>2</sub>, that can be produced by the interaction of A with LiNHAr<sup>Trip</sup> (Figure 2C). Single crystals of 1 were obtained by cooling a diethyl ether solution at -30 °C for two days. An X-ray diffraction study revealed that there are two crystallographically independent molecules in the unit cell, with similar structure metrics. As the representative, Figure 2B depicts the structure of one of the molecules. The three-coordinate Pd(I) complex has a P-Pd-P angle of 92.20(2)° and two unequal P-Pd-N angles of 108.06(6)° and  $154.04(6)^{\circ}$ . While the sum of the three angles  $(354.3^{\circ})$  indicates an idealized planar geometry for the Pd center, the presence of two unequal P-Pd-N angles differentiates 1 from trigonal-planar three-coordinate Pd(0) complexes (Pr<sub>2</sub>PCH<sub>2</sub>CH<sub>2</sub>CH<sub>2</sub>PPr<sub>2</sub>)Pd(PCy<sub>3</sub>)<sup>29</sup> and Pd(PPh<sub>3</sub>)<sub>3</sub>30 and T-shaped three-coordinate Pd(II) complexes  $(PBu_3^t)Pd(C_6H_4-4-OCH_3)(N(C_6H_3-3,5-(CF_3)_2)_2)^{31}$  $(IPr)Pd(3-methylnorborn-2-yl)(NHC_6H_4-4-CH_3)$  (IPr = 1,3-1)bis(2',6'-diisopropylphenyl)imidazole-2-ylidene).<sup>32</sup> bond distance in 1 is 2.063(2) Å, which is slightly longer than those of the three-coordinate Pd(II) amido complexes (sIPr)Pd(3-methylnorborn-2-yl)(NHC<sub>6</sub>H<sub>4</sub>-4-OCH<sub>3</sub>) (sIPr = 1,3-bis(2',6'-diisopropylphenyl)imidazolin-2-ylidene) (2.037(3) Å) and (IPr)Pd(3methylnorborn-2-yl)(NHC<sub>6</sub>H<sub>4</sub>-4-CH<sub>3</sub>) (2.011(3) Å).<sup>32</sup> Counter to the knowledge that the trans influence of the amido ligand would elongate the transoid Pd-P bond, the 2.2883(7) Å Pd1-P2 bond is shorter than the 2.3314(7) Å Pd1–P1 bond. The shortening of the Pd-P bond distance might be caused by the joint effect of Pd-tophosphine  $\pi$ -backdonation (*vide infra*) and the attractive dispersion forces between the phenyl groups on the P atom and the proximal 2,4,6-triisopropylphenyl group on the amido ligand (vide infra). In addition, the bond distances within the amido ligand of 1 itself are typical of anilido ligands in metal complexes, 31,32 and are different from those of the parent phenylaminyl radical [NHPh]. 33 and the arylaminyl complexes (Table S1),3437 which hints at the monoanionic nature of [NHAr<sup>Trip</sup>]<sup>1-</sup> in 1. Notably, the core structure of 1 is reminiscent of Hillhouse's nickel(I) amido

Spectroscopic and Electronic Structure Features of [(BINAP)Pd(NHAr<sup>Trip</sup>)]. Complex 1 features an  $S = \frac{1}{2}$  ground spin-state as indicated by the measured magnetic moment of 2.1(1) $\mu_{\rm B}$ . Continuous wave (CW) and field-swept echo-detected (FSE) EPR spectra were obtained for 1 (Figures 3A-3C, and S74). The Xband (9 GHz) CW-EPR spectrum obtained at room temperature shows a four-line pattern centered at  $g_{iso}$  ca. 2.052 with  $A_{iso}(^{31}\text{P1}) =$ 202 G (567 MHz) and  $A_{iso}(^{31}P2) = 80$  G (225 MHz) (Figure S74). The anisotropy of the g-values and the <sup>31</sup>P A-values were resolved at low temperatures by obtaining spectra at X-, Q- (35 GHz), and Wband (94 GHz). Figures 3A-3C shows the frozen-solution multifrequency EPR spectra obtained for 1 along with simulations using globally-fit spin Hamiltonian parameters. The g-values obtained are  $g_1 = 2.0085$ ,  $g_2 = 2.0350$ , and  $g_3 = 2.1115$ . The small g-value is consistent with the DFT-calculated electronic structure, as discussed below (Table 2), but is unusual among the few known Pd(I) complexes. For example, the spectra of the Pd(I) species generated by  $\gamma$ ray irradiation on Pd(II) compounds have their  $g_{\perp}$  values in the range 2.0 to 2.1 and  $g_{//}$  values in the range 2.1 to 2.6, 40 the spectrum of  $[(PBu_3^t)_2Pd][CB_{11}Cl_{11}H]$  has the *g*-values of  $g_{\perp} = 2.338$ ,  $g_{//} =$  $1.971_{1}^{19}$  and that of  $[(PBu_{3}^{t})_{2}Pd(NCMe)][CB_{11}Cl_{11}H]$  shows  $g_{\perp} =$  $2.088, g_{//} =$ 



**Figure 3.** Spectroscopic data of Pd complexes. (A-C) EPR spectra of **1** (black line) and simulations (red line) at 9 GHz CW, 34 GHz electron spin echo field sweep (derivative), and 94 GHz CW EPR. The minor features at the right in 94 GHz EPR spectrum comes from the Mn<sup>2+</sup> impurities from critoseal in W-band tube. (D) Overlay of the smoothed second derivatives of Pd K-edge XAS spectra of Pd<sup>0</sup>(IPr)<sub>2</sub> (**5**, blue), **1** (red), and (BINAP)Pd<sup>II</sup>(OAc)<sub>2</sub> (**6**, black). (E) Experimental (red) and TDDFT calculated (black) Pd L<sub>3</sub>-edge XAS spectra of **1**. The B3LYP functional and SARC-ZORA basis set was used for Pd, with ZORA-def2-TZVP(-f) used for all other atoms. Contributions of individual orbitals were obtained from Löwdin population analysis of the QROs. Orbitals are plotted at an isovalue of 0.03 au with hydrogen atoms removed for clarity.

Table 1. Experimental Pd K-Edge and L2,3-Edge Energies

	K-edge (eV)	L <sub>3</sub> pre-edge max (eV)	L <sub>2</sub> pre- edge max (eV)	Total $L_3 + L_2$ Mainline Area
5	24347	nd	nd	nd
1	24351	3174.5	3331.7	1.66(0.03)
6	24353	3176.4	3333.6	4.02(0.16)

2.314.<sup>19</sup> For the reference, EPR of Pd(III) generally display axial spectra with  $g_{//}$  and  $g_{\perp}$  values of 2.01-2.05 and 2.28-2.31, respectively, although isotropic and rhombic EPR spectra have also been reported.<sup>41</sup> The <sup>31</sup>P hyperfine constant values (HFCs) determined by globally fitting the frozen-solution EPR spectra of **1** for <sup>31</sup>P1 are:  $A_1 = 535$ ,  $A_2 = 535$ , and  $A_3 = 631$  MHz. The values for <sup>31</sup>P2 are  $A_1 = 205$ ,  $A_2 = 210$ , and  $A_3 = 260$  MHz. Deduction of atomic spin density from the isotropic ( $A_{iso}$ ) and dipolar (T) contributions to the HFCs<sup>42</sup> yields a spin density of 13.0% on P1, of which 4.3% resides in the 3s orbital and 8.7% in a 3p orbital, and a spin density on P2 is 6.4%, where 1.7% resides in the 3s orbital and 4.7% in the 3p orbital. Thus,

total spin density on two P nuclei is *ca.* 20 % based on the EPR experiments.  $A(^{105}\text{Pd})$  and  $A(^{14}\text{N})$  contributions to the spectra could not be resolved.

To probe the electronics of the Pd center in 1, Pd K- and L-edge XAS data for 1, the Pd(0) complex  $[Pd^{0}(IPr)_{2}]$  (5), and the Pd(II)complex  $[(BINAP)Pd^{II}(OAc)_2]$  (6) were collected. As shown in Figures 3D and S75, and Table 1, the rising-edge energies obtained from K-edge (1s  $\rightarrow$  valence/continuum) for the series of compounds shift toward higher energies with increasing formal oxidation state, though it has been noted that factors such as coordination environment and ligand identity can shift rising-edge energies to degrees similar to shifts caused by oxidation state changes. 43 Pre-edge features arising from the metal  $1s \rightarrow nd$  transitions are also conventionally used to assess physical oxidation states. Such excitations are not expected for the Pd(0) complexes because of their  $d^{10}$  configuration, but will occur in the case of formally Pd(I) and Pd(II) complexes. Such features are not resolved in the experimental Pd K-edge spectra likely owing to the weak intensity of these quadrupole allowed but dipole forbidden transitions as well as the core-hole lifetime broadening endemic to 2<sup>nd</sup> and 3<sup>rd</sup> row metal K-edge XAS.

To complement the *K*-edge data, the Pd  $L_{2,3}$ -edge (2p  $\rightarrow$  valence/continuum) XAS data were obtained, where dipole-allowed Pd  $2p \rightarrow 4d$  transitions gives rise to intense features that probe the

energetics and covalency of the Pd ligand field. Experimental Pd  $L_{2,3}$ -edge spectra are shown in Figures 3E and S75-S77 for 1 and 6. L<sub>3</sub> and L<sub>2</sub> mainlines in these spectra can be assigned to excitations from the Pd 2p orbitals into singly or unoccupied Pd 4d orbitals. Satellite features at higher energies relative to the mainline result from transitions into higher lying levels of primarily ligand character (*vide infra*). The  $L_3$  and  $L_2$  mainlines for 1 are shifted by ca. 2 eV to lower energy relative to 6 (Table 1). Areas of  $L_{2,3}$ -edge mainlines can be used to quantify metal nd character in valence acceptor orbitals, providing a direct probe of covalency and physical oxidation state. This approach has been applied to Pd  $L_{2,3}$ -edges, where an increase in the  $L_{2,3}$ -edge area of PdAl<sub>3</sub> and PdCl<sub>2</sub> compared to Pd metal was attributed to d-count depletion. In the present case, the total  $L_{2,3}$ -edge mainline area of 1 is ca. half that of 6, consistent with Pd-localized reduction.

Hybrid density functional theory (DFT) calculations were carried out to interrogate the electronic structure of 1. All calculations used the dispersion-corrected B3LYP-D3 hybrid density functional<sup>46,47</sup> with the segmented all-electron relativistically contracted (SARC)-ZORA basis on Pd<sup>48</sup> and ZORA-def2-TZVP(-f) basis set on all other atoms. All calculations used crystallographic coordinates. Veracity of the electronic structure calculations was judged by comparison of calculated spectroscopic parameters to experiment. Spin-Hamiltonian parameters calculated for 1 agree well with experiment (Table 2). Specifically, the g-values as well as the magnitudes and asymmetry of the <sup>31</sup>P HFCs are effectively reproduced by experiment. Calculated Mulliken spin densities comprise 9.5 % 3p and 3.9 % 3s on P1 and 5.7 % 3p and 2.7 % 3s on P2, in splendid agreement with analysis of the experimentally obtained HFCs (vide supra). The calculation yielded low 14N and 105Pd HFC values, consistent with the fact that these features are unresolved in the EPR data.

**Table 2. Experimental and DFT-calculated EPR Parameters for 1** 

	Experimental	Calculated <sup>a</sup>
g tensor	[2.0085, 2.0350, 2.1115]	[2.0216, 2.0408, 2.1065]
$A(^{31}P1) / MHz$	[205, 210, 260]	[237, 242, 298]
$A(^{31}P2) / MHz$	[535, 535, 631]	[535, 537, 650]
$A(^{105}\mathrm{Pd})$ / MHz	NR	[105, 31.1, 80.8]
$A(^{14}N) / MHz$	NR	[2.6, 3.3, 24.7]

<sup>a</sup>Calculations used crystallographic coordinates with the B3LYP hybrid density function, D3 correction for dispersion, the SARC-ZORA basis set on Pd, and the ZORA-def2-TZVP(-f) basis set on all other atoms.

The single-point DFT solutions were used as starting points for time-dependent DFT (TDDFT) calculations of the XAS data obtained for  $\mathbf{1}$  and  $\mathbf{6}$ . TDDFT has been used previously to calculate  $L_{2,3}$ -edge XAS spectra for second-row transition metals and was shown to adequately reproduce the structure of experimental  $L_3$ -

edges without including the contributions from spin-orbit coupling that yield the  $L_3$ - $L_2$  splitting. TDDFT reproduced the overall envelope of  $L_3$  features in the experimental spectra (Figures 3E and S80). The satellite features to higher energy of the  $L_3$  mainlines comprise transitions into ligand-localized molecular orbitals with minimal Pd 4d character. The mainline transition in 1 primarily comprises the Pd  $2p \rightarrow \text{SOMO}$  excitation, while for (BINAP)Pd<sup>II</sup>(OAc)<sub>2</sub> the mainline consists of the Pd 2p LUMO excitation as well as transitions to two additional low-lying MOs with ca. 10% contributions from Pd 4d orbitals. Calculated total Pd 4d character in all acceptor orbital holes against summed  $L_3$  and  $L_2$  mainline areas gives a correlation with  $R^2 = 0.97$  (Figure S82). Formally Pd<sup>II</sup> complex 1 exhibits 30% lower overall d vacancy than the Pd<sup>II</sup> complex, providing further support for metal-centered reduction relative to formally Pd<sup>II</sup>-containing 6.

The experimentally-validated DFT calculations indicate that 1 bears a three-electron two-center Pd–N  $\pi$ -bond, and its electronic configuration of can be described as  $(\pi_{d_{xx}+p_{xy}})^2(d_{z2},d_{xz},d_{z2},d_{x2-y2})^8(\pi^*_{d_{xx}})^2$  $_{p_{N}}$ )<sup>1</sup>. Löwdin orbital populations show that the SOMO is highly delocalized, although there is a substantial (40%) Pd 4d contribution consistent with the observed anisotropy in g-values obtained for 1 (Figure 4A). Major contributors to the SOMO come from the P-donors (10.3 % 3p) and the amide (10.4 % N 2p). The sum of the spin density on the NHAr<sup>Trip</sup> fragment, 0.22, precludes description of 1 as an aminyl radical complex. Relevant comparisons include the aminyl radical species  $[(bipy)Rh(N(Trop)_2)][OTf]$  (0.56, bipy = bipyri-Trop 5H-dibenzo[a,d ]cyclohepten-5-yl),<sup>26</sup> [(Ph<sub>2</sub>B(CH<sub>2</sub>PBu<sup>t</sup><sub>2</sub>)<sub>2</sub>)Cu(N(tolyl-p)<sub>2</sub>)] $(0.69)^{36}$  $[(Me_3NN)Cu(NPh_2)]$  (0.58,  $Me_3NN = 2,4-bis(2,4,6-trime$ thylphenylimido)pentyl),<sup>37</sup> [(PNP)NiCl][OTf] (0.69),<sup>35</sup> and  $[(PNP)Re(CO)_3][OTf]$  (0.83)<sup>34</sup> that feature higher spin density on their *N*-ligands. On the other hand, the spin-density distribution on 1 is more close to that of Hillhouse's Ni(I) amido complex [(dtbpe)Ni(NHDmp)],39 where the unpaired spin locates essentially on the nickel center (0.76 on nickel and 0.07 on nitrogen as shown in Figure S89).

To gain further insight into the nature of the Pd-N bond in **1**, we did bonding analysis by using the state-of-the-art energy decomposition analysis (EDA)<sup>50</sup> with the natural orbitals for chemical valency (NOCV) approach (see SI for details).<sup>51-53</sup> The most important numerical results are provided in Figure 4B, while the more detailed information can be found in Table S3 and Figures S84-S88. The interacting neutral fragments of (BINAP)Pd<sup>0</sup> and NHAr<sup>Trip</sup> has comparable orbital energy (i.e.,  $\Delta E_{\rm orb}$  = -72.0 kcal/mol) with that of the ionic fragments of [(BINAP)Pd<sup>1</sup>]<sup>+</sup> and [NHAr<sup>Trip</sup>]<sup>-</sup> (i.e.,  $\Delta E_{\rm orb}$  = -73.7 kcal/mol), implying the two resonant structures exist for **1** but the neutral fragments are slightly favored because of the smaller orbital energy (see Figure S88a). This also agrees very well with the spectroscopic data and spin density analysis as shown in Figure S88b. It revealed that there is significant Pauli

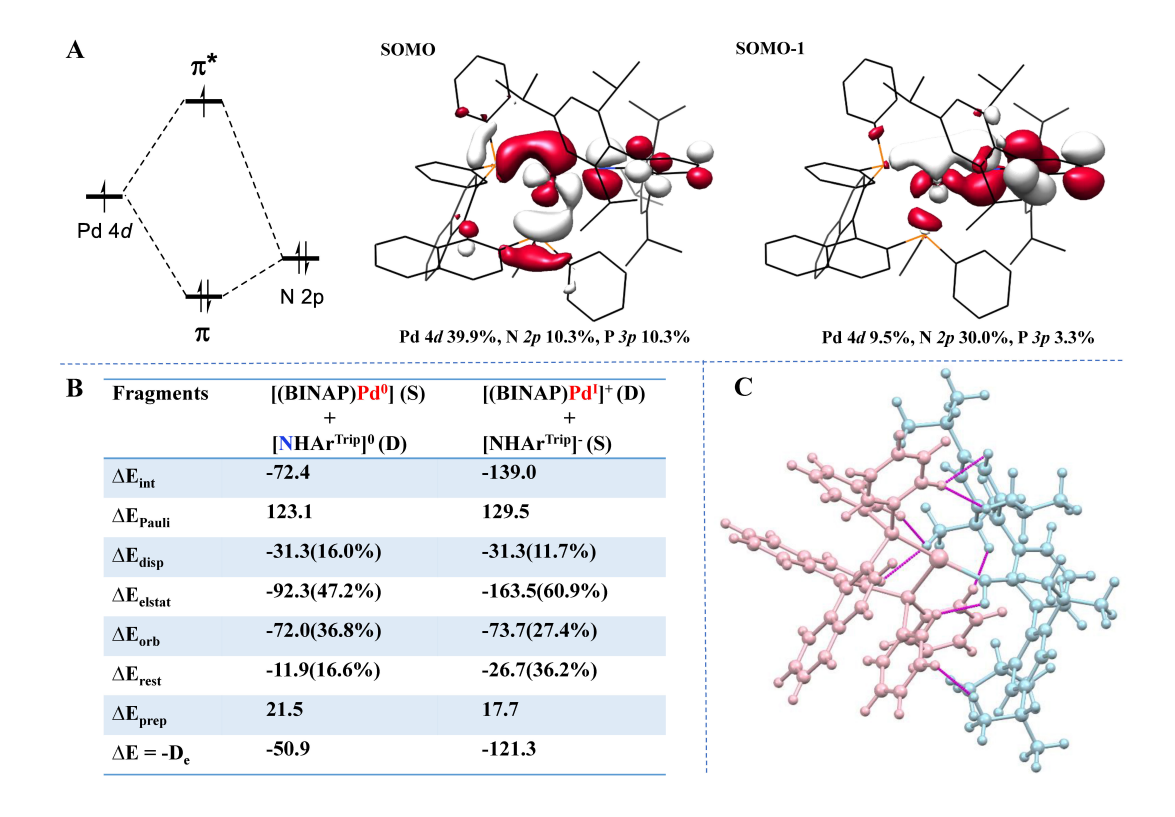


**Figure 4.** DFT calculations of Pd(I) amido complex. (A) Selected molecular orbitals of 1, hydrogen atoms on ligands were omitted. (B) EDA-NOCV results (in kcal/mol). Fragments of (BINAP)Pd and NHAr<sup>Trip</sup> are given on table in singlet (S) or doublet (D) electronic states. (C) Short inter-ligand H•••H contacts with the distances less than 2.4 Å (purple lines).

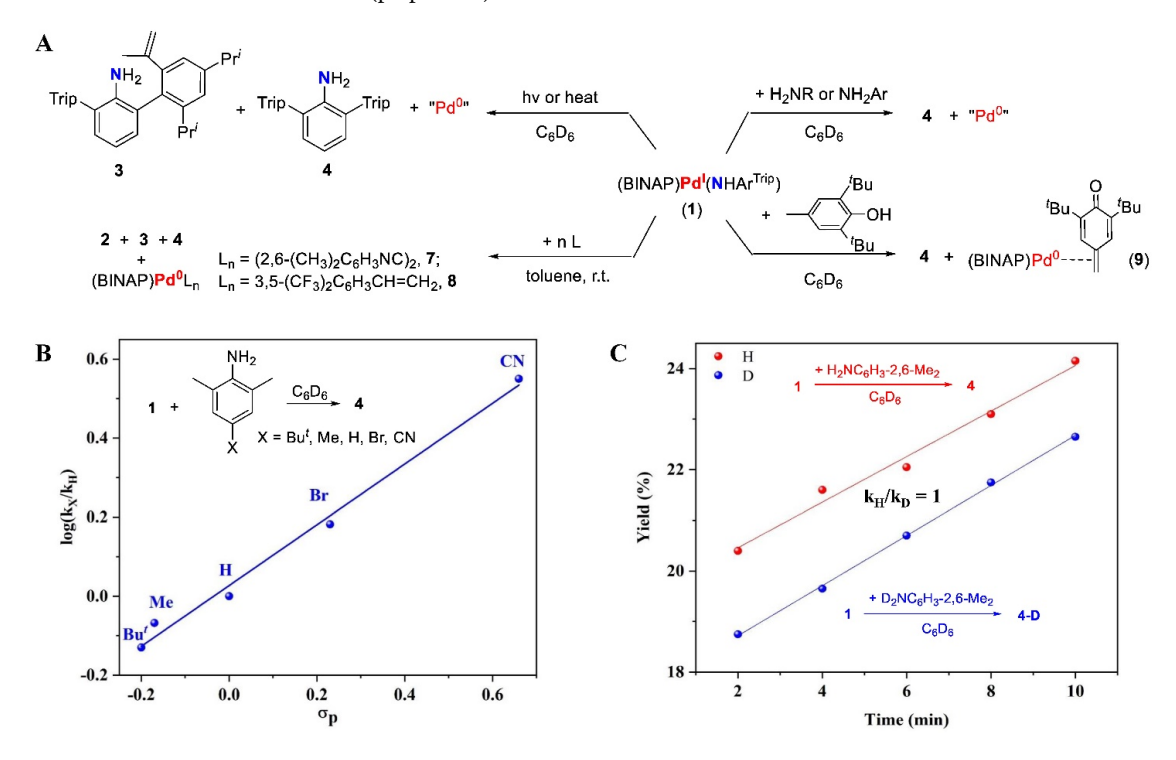


**Figure 5.** Reactivity of **1**. (A) Thermolysis-, light irradiation, and ligand-coordination-induced decomposition reactions of **1**, as well as its reactions with primary amines and a phenol. (B) The Hammett plot with *para*-substituted 2,6-dimethylaniline ( $k_{\rm X}/k_{\rm H}$  = relative rate constants for *para*-X substituted 2,6-dimethylanilines versus 2,6-dimethylaniline;  $\sigma_{\rm P}$  = Hammett substituent constant,  $\rho$  = reaction constant). (C) The kinetic isotope effect  $k_{\rm H}/k_{\rm D}$  for the reactions of **1** with 2,6-dimethylaniline.

repulsion (i.e.,  $\Delta E_{Pauli} = 123.1 \text{ kcal/mol}$ ) within the Pd–N interaction by using the neutral interacting fragments. Nonetheless, the favorable attractive interactions, including the electrostatic energy  $(\Delta E_{\text{elstat}} = -92.3 \text{ kcal/mol})$  and orbital interaction energy  $(\Delta E_{\text{orb}} = -$ 72.0 kcal/mol), can compensate and even exceeds the Pauli repulsion  $\Delta E_{\text{Pauli}}$  by 41.2 kcal/mol. It should be emphasized that the dispersion energy ( $\Delta E_{\text{disp}} = -31.3 \text{ kcal/mol}$ ) contributing 16% of total attractive forces, leads to a summed bond dissociation energy (D<sub>e</sub>) of 50.9 kcal/mol—help to stabilize the Pd(I) amido species at ambient temperature. The dispersion forces can be discerned from the short inter-ligand H...H contacts between BINAP and NHAr  $^{\text{Trip}}$  in the optimized structure of 1 (Figure 4C). The ionic interacting fragments has similar Pauli repulsion and orbital energies but with a significant strong electrostatic energy ( $\Delta E_{\text{elstat}} = -163.5$ kcal/mol), which is understandable between the cation [(BINAP)Pd<sup>1</sup>]+ and anion [NHAr<sup>Trip</sup>]- fragments and thus leads to more larger intrinsic energy  $\Delta E_{\rm int}$  of -139.0 kcal/mol and bond dissociation energy  $(D_e)$  of 121.3 kcal/mol. It should be mentioned that, in addition to the thermodynamic factors, the stabilization of 1 apparently benefits from steric protection of the Pd-N bond by the bulky substituents.

**Reactivity of** [(BINAP)Pd(NHAr<sup>Trip</sup>)]. Complex 1 is the first isolable  $d^9$  platinum-group-metal complex bearing a  $\pi$ -donating ligand. Being different from the aforementioned fleeting Pd(I) species, it is stable at ambient temperature, which facilitates studies of its reactivity. When 1 is subjected to thermolysis, light-irradiation, or coordination with exogenous ligands, it undergoes Pd–N bond homolytic cleavage reactions to yield anilines and Pd(0) species (Figure SA). In these reactions, the arylaminyl radical dimerization product 2, the alkane-chain dehydrogenation product 3 and the aniline NH<sub>2</sub>Ar<sup>Trip</sup> (4) are observed, implicating the radical intermediate [NHAr<sup>Trip</sup>] in these reactions (Figure S19). In addition, two Pd(0) complexes, [(BINAP)Pd(2,6-(CH<sub>3</sub>)<sub>2</sub>-C<sub>6</sub>H<sub>3</sub>NC)<sub>2</sub>] (7) and [(BINAP)Pd( $\eta^2$ -3,5-(CF<sub>3</sub>)<sub>2</sub>-C<sub>6</sub>H<sub>3</sub>CHCH<sub>2</sub>)] (8), have been isolated in the corresponding reaction and structurally authenticated by X-ray diffraction studies (Figures S29 and S34).

The decomposition reaction of 1 under white light-irradiation (6 W LED) at room temperature shows zero-order kinetics with a kinetic constant  $k_{irri} = 1.6 \times 10^{-8} \text{ mol} \cdot \text{L}^{-1} \cdot \text{s}^{-1}$  (Figure S23), whereas the thermal decomposition reaction at 348 K is a first-order reaction with a rate constant  $k_{therm} = 1.1 \times 10^{-4} \text{ s}^{-1}$  (Figure S27). The thermal and light-irradiation-induced decomposition reactions of 1 might result from amido-to-palladium(I) electron-transfer to form (BINAP)Pd<sup>0</sup>(NHAr<sup>Trip</sup>). The absorption spectrum of 1 in toluene shows an intense feature at 808 nm (7300 mol<sup>-1</sup>•L•cm<sup>-1</sup>). TDDFT calculations suggest that the band principally arises due to what is best described as a  $\pi \rightarrow \pi^*$  transition with ligand-to-metal charge transfer (LMCT) character: the principal donor orbital is the Pd-N  $\pi$ -bonding SOMO-1 whose largest contributor is the N 2p, while the acceptor orbital is the Pd-N  $\pi^*$  SOMO that is dominated by Pd 4d character (Figure S79). Either transition fully populates the Pd-N antibonding MO and thus promotes bond cleavage. Kinetics study on the reactions of 1 with an excess amount of 3,5-bis(trifluromethyl)styrene in benzene at 30 °C revealed pseudo-first-order kinetics on both the concentrations of 1 and the alkene (Figures S41-S47). This suggests that the ligand-coordination-induced-decomposition reaction might proceed via an associative mechanism or involve ligand exchange equilibria.

When 1 is treated with phenols and amines, e.g. 2,6-di(tert-butyl)-4-methylphenol, 2,6-di(iso-propyl)aniline, 2,6-dimethylaniline, nbutyl amine, and *n*-octyl amine, the free aniline  $NH_2Ar^{Trip}$  (4) was formed in high yields. The reaction with the phenol allows the isolation of a Pd(0) complex (2,6-di-tert-butyl-4-methylenecyclohexa-2,5-dienone)palldium(0) complex (9) in 67% yield (Figure 5A), whose structure has been confirmed by X-ray diffraction (Figures S48 and S49). The reactions with amines produced blue-purple mixtures and the attempts to isolate palladium-containing species from the mixture were unsuccessful. These reactions likely start with a proton-transfer step between the basic amido ligand in 1 and the H-X(X = O, N) bonds in phenols and amines, rather than a hydrogenatom-abstraction mechanism as i) a linear Hammett plot with a positive reaction constant  $\rho = +0.77$  was obtained for the reactions of 1 with anilines bearing different para-substituents (Figure 5B), ii) no obvious kinetic isotope effect was observed in the reactions 1 with 2,6-Me<sub>2</sub>C<sub>6</sub>H<sub>3</sub>NH<sub>2</sub> and 2,6-Me<sub>2</sub>C<sub>6</sub>H<sub>3</sub>ND<sub>2</sub> (Figure 5C), iii) no reaction took place when 1 was treated with substrates bearing weak C-H bonds, e.g. xanthene (73.3 kcal/mol in DMSO) and cyclohexa-1,4-diene (67 kcal/mol in gas phase), whose C-H bond dissociation energies are much lower than those of the O-H bond of 2,6-di(tertbutyl)-4-methylphenol (78 kcal/mol in DMSO) and the N-H bonds of amines (\$89 kcal/mol in DMSO).54 Thus, the formation of the Pd(0) complex **9** can be explained by the sequential steps of protontransfer followed by electron-transfer and hydrogen-atom abstraction reactions (Figure S55). Notably, as anilido anions are generally less basic than aliphatic amido anions,54 the capability of 1 to react with aliphatic amines to form NH<sub>2</sub>Ar<sup>Trip</sup> demonstrates the unique reactivity of the d9 Pd amido species. The elucidation of the mechanism of the reaction of 1 with aliphatic amines needs further study.

## Conclusion

In summary, the first isolable, room-temperature stable Pd(I) complex bearing an  $\pi$ -donating ligand [(BINAP)Pd(NHAr<sup>Trip</sup>)], which also represents the first platinum-group-metal amido complex with a nd9 electronic configuration, has been synthesized from the salt elimination reaction of (BINAP)PdCl<sub>2</sub> with LiNHAr<sup>Trip</sup>. The Pd(I) amido complex features a long Pd-N bond and inequivalent N-Pd-P angles. EPR and XAS spectroscopies indicate that Pd-N bond in the Pd(I) amido complex is highly covalent. Theoretical studies accord with the spectroscopic data and further revealed that pronounced dispersion forces between the BINAP and the bulky amido ligand NHAr<sup>Trip</sup> help the stabilization of this complex. Reacstudies revealed that the Pd-N bond [(BINAP)Pd(NHAr<sup>Trip</sup>)] can undergo homolytic cleavage reaction to release the aminyl radical [NHAr<sup>Trip</sup>] when the complex is subjected to heat, light-irradiation, or ligand-coordination. The Pd(I) complex can also react with primary amines to yield NH<sub>2</sub>Ar<sup>Trip</sup>. The reactivity profile of the Pd(I) amido complex points out the potential synthetic utility of low-valent platinum-group-metal species bearing  $\pi$ -donating ligands for the design of new reactions.

# **ASSOCIATED CONTENT**

# **Supporting Information**

The Supporting Information is available free of charge on the ACS Publications website at DOI: xxxxxxxxx.

Crystallographic data (CIF)

Experimental procedures, characterization, data, computational details, Cartesian coordinates (PDF)

# **AUTHOR INFORMATION**

# **Corresponding Author**

\* E-mails: shkim7@kbsi.re.kr (S.H.K), ias\_llzhao@njtech.edu.cn (L.Z.), kml236@cornell.edu (K.M.L.), deng@sioc.ac.cn (L.D.)

#### ORCID

Yujeong Kim: 0000-0001-7667-996X

Samantha N. MacMillan: 0000-0001-6516-1823

Xuebing Leng: 0000-0003-3291-8695 Sun Hee Kim: 0000-0001-6557-1996 Lili Zhao: 0000-0003-2580-6919

Kyle M. Lancaster: 0000-0001-7296-128X Liang Deng: 0000-0002-0964-9426

# **Author Contributions**

The manuscript was written through contributions of all authors. All authors have given approval to the final version of the manuscript.

#### Notes

The authors declare no competing financial interests.

## ACKNOWLEDGMENT

We thank Mr. Chenglu Lu for the cold electron spray mass spectrometry measurements, and Mr. Jianfeng Zhang for elemental analysis. L.D. thanks the financial support from the National Natural Science Foundation of China (grants 21725104, 21690062, 22061160464, and 21821002), the Science and Technology Commission of Shanghai Municipality (grant 19XD1424800), and K. C. Wong Education Foundation. K.M.L. thanks the NSF for support of this research via CHE-1954515. M.M.B is an NSF Graduate Research Fellow. XAS data were obtained at SSRL, which is supported by the DOE, Office of Science, Office of Basic Energy Sciences under Contract No. DE-AC02-76SF00515. The SSRL Structural Molecular Biology Program is supported by the US DOE Office of Biological and Environmental Research, and by NIH/NIGMS (including P41GM103393). S.H.K. thanks the NRF of Korea for support of this research (NRF-2017M3D1A1039380). L.Z. thanks the financial support from National Natural Science Foundation of China (Grant No. 21973044), the State Key Laboratory of Materials-oriented Chemical Engineering (project No. KL19-11), and the high performance center of Nanjing Tech University for supporting the computational resources.

# REFERENCES

- 1. Hartings, M. Reactions coupled to palladium. Nat. Chem. 2012, 4, 764.
- 2. Powers, D. C.; Ritter, T. Palladium(III) in synthesis and catalysis. *Top. Organomet. Chem.* **2011**, *503*, 129-156.
- 3. Liu, Q.; Dong, X.; Li, J.; Xiao, J.; Dong, Y.; Liu, H. Recent advances on palladium radical involved reactions. ACS Catal. 2015, 5, 6111-6137.
- 4. Bonney, K. J.; Proutiere, F.; Schoenebeck, F. Dinuclear Pd(I) complexes-solely precatalysts? Demonstration of direct reactivity of a Pd(I) dimer with an aryl iodide. *Chem. Sci.* **2013**, *4*, 4434-4439.
- 5. Cui, P.; Iluc, V. M. Redox-induced umpolung of transition metal carbenes. *Chem. Sci.* **2015**, *6*, 7343-7354.
- 6. Parasram, M.; Chuentragool, P.; Sarkar, D.; Gevorgyan, V. Photoinduced formation of hybrid aryl Pd-radical species capable of 1,5-HAT: Selective catalytic oxidation of silyl ethers into silyl enol ethers. *J. Am. Chem. Soc.* **2016**, *138*, 6340-6343.
- 7. Zhao, B.; Shang, R.; Wang, G.-Z.; Wang, S.; Chen, H.; Fu, Y. Palladium-catalyzed dual ligand-enabled alkylation of silyl enol ether and enamide

- under irradiation: Scope, mechanism, and theoretical elucidation of hybrid alkyl Pd(I)-radical species. ACS Catal. 2019, 10, 1334-1343.
- 8. Torres, G. M.; Liu, Y.; Arndtsen, B. A. A dual light-driven palladium catalyst: Breaking the barriers in carbonylation reactions. *Science.* **2020**, *368*, 318-323.
- 9. Chen, Q.-Y.; Yang, Z.-Y.; Zhao, C.-X.; Qiu, Z.-M. Studies on fluoroalkylation and fluoroalkoxylation. Part 28. Palladium(0)-induced addition of fluoroalkyl iodides to alkenes: an electron transfer process. *J. Chem. Soc., Perkin Trans.* 1988, 1, 563-567.
- 10. Jaworski, J. N.; McCann, S. D.; Guzei, I. A.; Stahl, S. S. Detection of palladium(I) in aerobic oxidation catalysis. *Angew. Chem., Int. Ed.* **2017**, *56*, 3605-3610.
- 11. Fafard, C. M.; Adhikari, D.; Foxman, B. M.; Mindiola, D. J.; Ozerov, O. V. Addition of ammonia, water, and dihydrogen across a single Pd-Pd bond. *J. Am. Chem. Soc.* **2007**, *129*, 10318-10319.
- 12. Fujiwara, S.; Nakamura, M. Electron spin resonance of Pd(I). I.  $\gamma$ -irradiated bis(acetylacetonato)palladium(II). *J. Chem. Phys.* **1970**, *52*, 6299-6301
- 13. Fujiwara, S.; Nakamura, M. Electron spin resonance of Pd(I). II.  $\gamma$ -irradiated single crystals of  $K_2PdCl_4$  and  $(NH_4)_2PdCl_4$ . J. Chem. Phys. **1970**, 54. 3378-3380
- 14. Taarit, Y. B.; Vedrine, J. C.; Dutel, J. F.; Naccache, C. Epr investigation of structure and reactivity of Pd(I) species generated in synthetic mordenite-type zeolite. *J. Magn. Reson.* **1978**, *31*, 251-257.
- 15. Lane, G. A.; Geiger, W. E.; Connelly, N. G. Palladium(I) .pi.-radicals. Electrochemical preparation and study of their reaction pathways. *J. Am. Chem. Soc.* **1987**, *109*, 402-407.
- 16. Luo, J.; Tran, G. N.; Rath, N. P.; Mirica, L. M. Detection and characterization of mononuclear Pd(I) complexes supported by N2S2 and N4 tetradentate ligands. *Inorg. Chem.* **2020**, *59*, 15659-15669.
- 17. Blake, A. J.; Gould, R. O.; Hyde, T. I.; Schröder, M. Stabilisation of monovalent palladium by tetra-aza macrocycles. *J. Chem. Soc., Chem. Commun.* **1987**, *0*, 431-433.
- 18. Troadec, T.; Tan, S. Y.; Wedge, C. J.; Rourke, J. P.; Unwin, P. R.; Chaplin, A. B. One-electron oxidation of  $[M(P^tBu_3)_2]$  (M=Pd, Pt): Isolation of monomeric  $[Pd(P^tBu_3)_2]^+$  and redox-promoted C-H Bond cyclometalation. *Angew. Chem., Int. Ed.* **2016**, *55*, 3754-3757.
- 19. MacInnis, M. C.; DeMott, J. C.; Zolnhofer, E. M.; Zhou, J.; Meyer, K.; Hughes, R. P.; Ozerov, O. V. Cationic two-coordinate complexes of Pd(I) and Pt(I) have longer metal-ligand bonds than their neutral counterparts. *Chem.* **2016**, *1*, 902-920.
- 20. Bickelhaupt, F. M.; Jan Baerends, E. Kohn-Sham density functional theory: Predicting and understanding chemistry. *Rev. Comput. Chem.* **2000**, *15*, 1-86.
- 21. Caulton, K. G. The influence of Pi-stabilized unsaturation and filled repulsions in transition-metal chemistry. *New J. Chem.* **1994**, *18*, 25-41.
- 22. Bryndza, H. E.; Tam, W. Monomeric metal hydroxides, alkoxides, and amides of the late transition metals: synthesis, reactions, and thermochemistry. *Chem. Rev.* **1988**, *88*, 1163-1188.
- 23. Fulton, J. R.; Holland, A. W.; Fox, D. J.; Bergman, R. G. Formation, reactivity, and properties of nondative late transition metal–oxygen and –nitrogen bonds. *Acc. Chem. Res.* **2002**, *35*, 44-56.
- 24. Gunnoe, T. B. Reactivity of ruthenium(II) and copper(I) complexes that possess anionic heteroatomic ligands: Synthetic exploitation of nucleophilicity and basicity of amido, hydroxo, alkoxo, and aryloxo ligands for the activation of substrates that possess polar bonds as well as nonpolar C–H and H–H bonds. *Eur. J. Inorg. Chem.* **2007**, 1185-1203.
- Fryzuk, M. D.; Montgomery, C. D. Amides of the platinum group metals. Coord. Chem. Rev. 1989, 95, 1-40.
- 26. Buttner, T.; Geier, J.; Frison, G., Harmer, J.; Calle, C.; Schweiger, A.; Schonberg, H.; Grutzmacher, H. A stable aminyl radical metal complex. *Science.* **2005**, *307*, 235-238.
- 27. Driver, M. S.; Hartwig, J. F. A rare, low-valent alkylamido complex, a diphenylamido complex, and their reductive elimination of amines by three-coordinate intermediates. *J. Am. Chem. Soc.* **1995**, *117*, 4708-4709.
- 28. Liptrot, D. J.; Power, P. P. London dispersion forces in sterically crowded inorganic and organometallic molecules. *Nat. Rev. Chem.* **2017**, *1*, 1-12.

- 29. Perez, P. J.; Calabrese, J. C.; Bunel, E. E. Synthesis, characterization, and reactivity of  $[(({}^iPr)_2P(CH_2)_3P({}^iPr)_2)(PCy_3)PdH][OR]$ . Organometallics **2001**, 20, 337-345.
- 30. Tejel, C.; Asensio, L.; del Rio, M. P.; de Bruin, B.; Lopez, J. A.; Ciriano, M. A. Developing synthetic approaches with non-innocent metalloligands: easy access to Ir(I)/Pd(0) and Ir(I)/Pd(0)/Ir(I) cores. *Angew. Chem., Int. Ed.* **2011**, *50*, 8839-8843.
- 31. Yamashita, M.; Hartwig, J. F. Synthesis, structure, and reductive elimination chemistry of three-coordinate arylpalladium amido complexes. *J. Am. Chem. Soc.* **2004**, *126*, 5344-5345.
- 32. Hanley, P. S.; Marquard, S. L.; Cundari, T. R.; Hartwig, J. F. Reductive elimination of alkylamines from low-valent, alkylpalladium(II) amido complexes. *J. Am. Chem. Soc.* **2012**, *134*, 15281-15284.
- 33. Penkert, F. N.; Weyhermüller, T.; Bill, E.; Hildebrandt, P.; Lecomte, S.; Wieghardt, K. Anilino radical complexes of cobalt(III) and manganese(IV) and comparison with their phenoxyl analogues. *J. Am. Chem. Soc.* **2000**, *122*, 9663-9673.
- 34. Radosevich, A. T.; Melnick, J. G.; Stoian, S. A.; Bacciu, D.; Chen, C. H.; Foxman, B. M.; Ozerov, O. V.; Nocera, D. G. Ligand reactivity in diarylamido/bis(phosphine) PNP complexes of Mn(CO)<sub>3</sub> and Re(CO)<sub>3</sub>. *Inorg. Chem.* **2009**, 48, 9214-9221.
- 35. Adhikari, D.; Mossin, S.; Basuli, F.; Huffman, J. C.; Szilagyi, R. K.; Meyer, K.; Mindiola, D. J. Structural, spectroscopic, and theoretical elucidation of a redox-active pincer-type ancillary applied in catalysis. *J. Am. Chem. Soc.* **2008**, *130*, 3676-3682.
- 36. Mankad, N. P.; Antholine, W. E.; Szilagyi, R. K.; Peters, J. C. Three-coordinate copper(I) amido and aminyl radical complexes. *J. Am. Chem. Soc.* **2009**, *131*, 3878-3880.
- 37. Wiese, S.; Badiei, Y. M.; Gephart, R. T.; Mossin, S.; Varonka, M. S.; Melzer, M. M.; Meyer, K.; Cundari, T. R.; Warren, T. H. Catalytic C-H amination with unactivated amines through copper(II) amides. *Angew. Chem., Int. Ed.* **2010**, *49*, 8850-8855.
- 38. Mindiola, D. J.; Hillhouse, G. L. Terminal amido and imido complexes of three-coordinate nickel. *J. Am. Chem. Soc.* **2001**, 123, 4623-4624.
- 39. Iluc, V. M.; Hillhouse, G. L. Hydrogen-atom abstraction from Ni(I) phosphido and amido complexes gives phosphinidene and imide ligands. *J. Am. Chem. Soc.* **2010**, *132*, 15148-15150.
- 40. Nakamura, M.; Fujiwara, S. Electron spin resonance of Pd(I). III\* The nature of the metal-ligand bonds in square planar complexes of palladium(I). *J. Coord. Chem.* **1972**, *1*, 221-227.
- 41. Khusnutdinova, J. R.; Rath, N. P.; Mirica, L. M. Stable mononuclear organometallic Pd(III) complexes and their C-C bond formation reactivity. *J. Am. Chem. Soc.* **2010**, *132*, 7303-7305.

- 42. Morton, J. R.; Preston, K. F. Atomic parameters for paramagnetic resonance data. *J. Magn. Reson.* **1978**, *30*, 577-582.
- 43. MacMillan, S. N.; Lancaster, K. M. X-ray spectroscopic interrogation of transition-metal-mediated homogeneous catalysis: Primer and case studies. *ACS Catal.* **2017**, *7*, 1776-1791.
- 44. Boysen, R. B.; Szilagyi, R. K. Development of palladium L-edge X-ray absorption spectroscopy and its application for chloropalladium complexes. *Inorg. Chim. Acta.* **2008**, *361*, 1047-1058.
- 45. Sham, T. K. L-edge x-ray-absorption spectra of PdAl<sub>3</sub> and PdCl<sub>2</sub>: A study of charge redistribution in compounds of an element with a nearly full 4d shell. *Phys. Rev. B.* **1985**, *31*, 1903-1908.
- 46. Elstner, M.; Hobza, P.; Frauenheim, T.; Suhai, S.; Kaxiras, E. Hydrogen bonding and stacking interactions of nucleic acid base pairs: A density-functional-theory based treatment. *J. Chem. Phys.* **2001**, *114*, 5149-5155
- 47. Grimme, S.; Antony, J.; Ehrlich, S.; Krieg, H. A consistent and accurate ab initio parametrization of density functional dispersion correction (DFT-D) for the 94 elements H-Pu. *J. Chem. Phys.* **2010**, *132*, 154104.
- 48. Rolfes, J. D.; Neese, F.; Pantazis, D. A. All-electron scalar relativistic basis sets for the elements Rb-Xe. J. Comput. Chem. **2020**, 41, 1842-1849.
- 49. He, W.; Kennepohl, P. Direct experimental evaluation of ligand-induced backbonding in nickel metallacyclic complexes. *Faraday Discuss* **2019**, 220, 133-143.
- 50. Ziegler, T.; Rauk, A. On the calculation of bonding energies by the Hartree Fock Slater method. *Theoret. Chim. Acta.* **1977**, *46*, 1-10.
- 51. Mitoraj, M.; Michalak, A. Donor–acceptor properties of ligands from the natural orbitals for chemical valence. *Organometallics* **2007**, *26*, 6576-6580.
- 52. Mitoraj, M.; Michalak, A. Applications of natural orbitals for chemical valence in a description of bonding in conjugated molecules. *J. Mol. Model.* **2008**, *14*, 681-687.
- 53. Mitoraj, M.; Michalak, A.; Ziegler, T. A combined charge and energy decomposition scheme for bond analysis. *J. Chem. Theory Comput.* **2009**, *5*, 962-975.
- 54. Warren, J. J.; Tronic, T. A.; Mayer, J. M. Thermochemistry of proton-coupled electron transfer reagents and its implications. *Chem. Rev.* **2010**, *110*, 6961-7001.

